



Published in final edited form as:

*Nat Genet.* 2019 June ; 51(6): 941–946. doi:10.1038/s41588-019-0428-5.

## Phosphorylation of histone H3.3 at serine 31 promotes p300 activity and enhancer acetylation

Sara Martire, Aishwarya A. Gogate, Amanda Whitmill, Amanuel Tafessu, Jennifer Nguyen, Yu-Ching Teng, Melodi Tastemel, and Laura A. Banaszynski\*

Cecil H. and Ida Green Center for Reproductive Biology Sciences and the Division of Basic Research, Department of Obstetrics and Gynecology, Children's Medical Center Research Institute, Hamon Center for Regenerative Medicine, University of Texas Southwestern Medical Center, Dallas, Texas 75390, USA.

### Abstract

The histone variant H3.3 is enriched at enhancers and active genes, as well as repeat regions such as telomeres and retroelements, in mouse embryonic stem cells (mESCs)<sup>1–3</sup>. While recent studies demonstrate a role for H3.3 and its chaperones in establishing heterochromatin at repeat regions<sup>4–8</sup>, the function of H3.3 in transcription regulation has been less clear<sup>9–16</sup>. Here, we find that H3.3-specific phosphorylation<sup>17–19</sup> stimulates activity of the acetyltransferase p300 in *trans*, suggesting that H3.3 acts as a nucleosomal cofactor for p300. Depletion of H3.3 from mESCs reduces acetylation on histone H3 at lysine 27 (H3K27ac) at enhancers. Cells lacking H3.3 demonstrate reduced capacity to acetylate enhancers that are activated upon differentiation, along with reduced ability to reprogram cell fate. Our study demonstrates that a single amino acid in a histone variant can integrate signaling information and globally impact genome regulation, which may help better understand how mutations in these proteins contribute to human cancers<sup>20,21</sup>.

### MAIN

The histone variant H3.3 was first identified as a component of active chromatin, and genome-wide studies suggest that at least 75% of H3.3 deposition occurs at regions associated with active genes in mESCs<sup>5</sup>. While it is known that H3.3 is enriched at active enhancers and genes, it is debatable whether its deposition at these regions is functionally required or simply a byproduct of the high levels of nucleosome turnover these regions experience<sup>4,9–16</sup>. As H3.3 is an integral nucleosomal component of enhancers (Fig. 1a and Supplementary Fig. 1a), we wanted to understand how its loss might affect the chromatin signature at these regions. Intriguingly, we found that mESCs lacking H3.3 (H3.3 KO)<sup>4</sup>

Users may view, print, copy, and download text and data-mine the content in such documents, for the purposes of academic research, subject always to the full Conditions of use: [http://www.nature.com/authors/editorial\\_policies/license.html#terms](http://www.nature.com/authors/editorial_policies/license.html#terms)

\*Correspondence: [laura.banaszynski@utsouthwestern.edu](mailto:laura.banaszynski@utsouthwestern.edu).

Author contributions

S.M. and L.A.B. conceived and designed the study; S.M. performed experiments with help from A.T., J.N., Y.-C.T. and M.T.; A.A.G. performed computational analyses; A.W. contributed to the differentiation study; L.A.B. supervised the project; S.M. and L.A.B. wrote the manuscript with input from all co-authors.

Competing interests

Authors declare no competing interests.

show a global reduction of H3K27ac without any appreciable reduction in H3K4me1 (Fig. 1b and Supplementary Fig. 1b–d). Mass spectrometry confirmed that the overall level of H3.1K27ac in H3.3 KO mESCs was ~60% of that in wild-type mESCs (Fig. 1c). Reduced acetylation was accompanied by an increase in global H3.1K27me2/3 (Supplementary Fig. 1e)<sup>22</sup>.

To explore the relationship between H3.3 and chromatin signatures at regulatory elements genome-wide, we performed chromatin immunoprecipitation followed by sequencing (ChIP-seq) of several histone modifications in wild-type and H3.3 KO mESCs. Inspection of genes encoding three pluripotency transcription factors, *Sox2*, *Pou5f1*, and *Nanog*, showed that the regulatory elements controlling these genes (indicated in gray and evidenced by binding of Oct4<sup>23</sup>, Nanog<sup>23</sup>, and p300) were marked by reduced levels of H3K27ac in the absence of H3.3 (Fig. 1d). Genome-wide, we found that the majority (13,135/17,589, ~75%) of promoter-distal enhancers marked by both H3K27ac and p300 showed reduced H3K27ac enrichment in the absence of H3.3 (Fig. 1e and Supplementary Fig. 1f–h). We confirmed these results in an independent ChIP-qPCR experiment at 16 individual enhancers in two H3.3 KO clonal mESCs (Supplementary Fig. 1i,j). Reduced acetylation was more pronounced at promoter-distal enhancers than at promoters themselves (Supplementary Fig. 1k). Reduced acetylation was not limited to H3K27ac, as H3K18ac, H3K64ac, and H3K122ac<sup>24</sup> also showed reduced levels at enhancers in H3.3 KO mESCs (Supplementary Fig. 1l–n). We did not observe an appreciable reduction in H3K4me1 at enhancers (Supplementary Fig. 1o,p). In line with the model of enhancer priming<sup>25–28</sup>, these results suggest that H3K4me1 is upstream of enhancer acetylation.

We next considered the two independent chaperone systems that deposit H3.3 into distinct regions of chromatin. The HIRA complex is responsible for the majority of genic deposition (i.e., promoters, gene bodies, and enhancers), while the ATRX/DAXX complex deposits H3.3 at repeat regions such as telomeres and interstitial heterochromatin (Supplementary Fig. 2a,b)<sup>2</sup>. We therefore predicted that loss of HIRA, but not ATRX or DAXX, would result in similar loss of enhancer acetylation as observed upon loss of H3.3. In support, we observed both a global reduction and enhancer-specific loss of H3K27ac in HIRA KO mESCs (Supplementary Fig. 2c,d). The vast majority of these regions (7,950/8,476, 94%) also showed reduced H3K27ac in H3.3 KO mESCs (Supplementary Fig. 2e). In contrast, ATRX KO did not alter H3K27ac enrichment and DAXX KO resulted in increased H3K27ac at enhancers in mESCs (Supplementary Fig. 2f). We then generated an independent HIRA KO mESC line that was isogenic with the ATRX and DAXX KO mESCs used in our study (Supplementary Fig. 2g). The reduction of H3K27ac at enhancers observed for these two independent HIRA KO mESCs was strikingly similar (Supplementary Fig. 2h,i) and consistent across independent experiments (Supplementary Fig. 2j). Overall, these data suggest that HIRA-dependent deposition of H3.3 at enhancers plays a role in maintaining histone acetylation of these regions.

We next wanted to understand how loss of H3.3 leads to changes in H3K27ac at regulatory elements. We did not detect changes in acetyl-CoA levels or increased histone deacetylase (HDAC) activity in H3.3 KO mESCs (Supplementary Fig. 3a,b). Further, we did not observe appreciable difference in expression of the p300 or CBP histone acetyltransferases

(Supplementary Fig. 3c). Since our data and others suggest that p300 is responsible for the majority of H3K27ac in mESCs (Supplementary Fig. 3d)<sup>22</sup>, we focused our attention on p300. To test whether reduced acetylation in the absence of H3.3 could be attributed to changes in chromatin accessibility and/or p300 recruitment, we performed ATAC-seq (Assay for Transposase-Accessible Chromatin using sequencing)<sup>29</sup> and ChIP-seq of p300 in WT and H3.3 KO mESCs. Surprisingly, we found that loss of H3.3 at enhancers did not dramatically reduce the “open” state nor p300 enrichment at enhancers in mESCs, especially compared to the reduced acetylation observed at these regions (Supplementary Fig. 3e,f).

Together, these observations suggest that some unique feature of H3.3 promotes p300 enzymatic activity. We considered the sequence of the H3.1/2 and H3.3 tails, which differ by only one amino acid. While canonical H3 contains an alanine at position 31, this residue in H3.3 is a serine that is a reported site of phosphorylation (H3.3S31ph, Fig. 2a)<sup>17–19</sup>. Since previous studies demonstrate that serine phosphorylation on histone tails can affect the acetylation of nearby lysines<sup>30,31</sup>, we wanted to test whether H3.3S31ph could enhance p300 activity in mESCs. We first exogenously expressed various histones or mutations thereof in H3.3 KO mESCs to determine their effect on H3K27ac levels. ChIP-qPCR confirmed that while both exogenous H3.3 and H3.2 were deposited at enhancers, only H3.3 restored H3K27ac levels to those observed in wild-type mESCs (Fig. 2b and Supplementary Fig. 4a). To test the role of H3.3S31 and its phosphorylation, we introduced exogenous H3.3 proteins with point mutations at this residue (H3.3S31A and H3.3S31E) into H3.3 KO mESCs (Fig. 2b and Supplementary Fig. 4b). We found that exogenous H3.3S31E expression (which mimics phosphorylation), but not H3.3S31A (which cannot be phosphorylated), resulted in recovery of H3K27ac levels comparable to those found in wild-type mESCs. Exogenous expression of either H3.3 or H3.3S31E in H3.3 KO mESCs also resulted in greater H3K27ac levels at enhancers compared to either H3.2 or H3.3S31A (Fig. 2c). Both H3.3S28A and H3.3S28E mutants were able to rescue global H3K27ac levels, suggesting that H3.3S31 phosphorylation may play a more important role than H3.3S28ph in stimulating p300 activity in mESCs (Supplementary Fig. 4b). Surprisingly, we found that expression of exogenous H3.3K27A in H3.3 KO mESCs was sufficient to increase acetylation levels (Fig. 2b). As this exogenous H3 protein cannot be acetylated at K27, this increase in H3K27ac must occur on the endogenous, canonical H3 protein, suggesting that H3.3 and/or its phosphorylation stimulates p300 activity in *trans*.

The above data suggest a model that requires physiological H3.3S31ph at enhancers. Given that previous reports demonstrate H3.3S31ph enrichment at telomeres<sup>17</sup> and mitotic centromeres<sup>18</sup> mediated by the kinase, Checkpoint Kinase 1 (Chk1)<sup>19</sup>, we wanted to determine the genome-wide enrichment profile of H3.3S31ph in cycling mESCs. Using ChIP-seq, we identified 11,259 regions of H3.3S31ph that were largely dependent on Chk1 activity (Supplementary Fig. 4c–e). More than half of H3.3S31ph-enriched regions ( $n = 5,755/11,259$ ) overlap with regions enriched with H3K27ac in our wild-type ESCs. Further, we find that H3.3S31ph is enriched at active mESC enhancers and is dependent on HIRA (Fig. 2d and Supplementary Fig. 4f). To further test the importance of phosphorylation in promoting p300 activity, we treated wild-type mESCs with either an inhibitor of Chk1 (Chk1i) or an inhibitor of the Aurora B kinase (Aurora Bi), another kinase implicated in H3.3 phosphorylation<sup>32</sup>. Treatment with Aurora Bi did not decrease H3.3S31ph levels and

instead resulted in reduced H3S28ph over time with little effect on H3K27ac (Fig. 2e,f and Supplementary Fig. 4g). Treatment with Chk1i reduced global levels of H3.3S31ph without inhibiting H3S28ph (Supplementary Fig. 4g). In support of phosphorylation-dependent p300 activation, Chk1 inhibition resulted in reduced H3K27ac at enhancers similar to the reductions observed in the H3.3 KO ESCs (Fig. 2e,f and Supplementary Fig. 4g,h). Treatment of H3.3 KO mESCs with Chk1i resulted in little further decrease in H3K27ac levels at enhancers (Fig. 2f), suggesting a connection between H3.3 phosphorylation and Chk1 in promoting p300 activity.

Finally, we performed *in vitro* analysis to determine the mechanistic effect of histone phosphorylation on p300 activity. We treated *in vitro* reconstituted mononucleosomes containing H3.3 with Chk1, resulting in phosphorylation on both S28 and S31 (Supplementary Fig. 5a). Phosphorylated nucleosomes stimulated p300 activity, resulting in higher levels of acetylation (Fig. 3a). To investigate the role of S31ph, we repeated this assay using H3.1-containing nucleosomes, which contain an alanine at position 31. We found that both H3.1 and H3.3 mononucleosomes were substrates for p300 *in vitro*, but only phosphorylated H3.3 nucleosomes resulted in an increase in p300 activity compared to the unphosphorylated substrate (Supplementary Fig. 5a,b). Since our cellular data suggest that this stimulation occurs in *trans* (see Figs. 1c and 2b), we tested whether phosphorylated nucleosomes containing H3.3 could stimulate p300 activity on unphosphorylated canonical nucleosomes (Fig. 3b). Using mass spectrometry, we found that the presence of phosphorylated H3.3 nucleosomes resulted in increased acetylation on canonical H3 (Fig. 3c). Overall, these data support a role for H3.3 phosphorylation in stimulating p300 activity in *trans* (Fig. 3d).

Since histone acetylation is correlated with gene expression, we compared transcription levels (RNA-seq) from equal numbers of wild-type and H3.3 KO mESCs using synthetic spike-in standards. Despite global reduction of H3K27ac (Fig. 1), we did not observe global reduction of transcription in H3.3 KO compared to wild-type ESCs (Supplementary Fig. 6a). We next compared up- and downregulated gene sets to the nearest neighboring genes of enhancers affected by H3.3 loss in mESCs (Supplementary Fig. 6b). While genes with increased nearby acetylation generally showed increased transcription (480/1,051, 46%), only 12% (344/2,796) of genes with decreased nearby acetylation showed significantly reduced transcription in H3.3 KO mESCs. We observed a similar relationship between enhancer acetylation and steady state transcription in HIRA KO mESCs (Supplementary Fig. 6c–f). Overall, these results suggest that reduced enhancer acetylation is well tolerated in mESCs (Supplementary Fig. 6g–i).

Since many latent enhancers are activated during differentiation, we wanted to address whether H3.3 is needed to establish acetylation during enhancer activation. We performed ChIP-seq of H3K27ac in wild-type and H3.3 KO cells that had been differentiated for four days into embryoid bodies (EBs). Genome-wide, we identified 2,054 enhancer sites (“EB enhancers”) that significantly gained H3K27ac in wild-type differentiated cells compared to mESCs and were not pre-bound by p300 in mESCs (Fig. 4a and Supplementary Fig. 7a). These regions did not show appreciable gains in H3K27ac in differentiating cells lacking H3.3 (Fig. 4a). Further, these enhancers remain “closed” in the absence of H3.3, suggesting

an early and fundamental role for H3.3 in activating latent enhancers (Fig. 4b). Unlike mESCs, differentiating cells were greatly affected by loss of H3.3, as nearest neighboring genes showed reduced transcription in H3.3-deleted EBs compared to wild-type EBs (Fig. 4c). In agreement with reduced enhancer activation and associated transcription, and in line with a role for H3.3 during development<sup>9</sup>, we found that H3.3 KO mESCs displayed delayed or defective differentiation, evidenced both by morphology and an inability to switch from a pluripotency transcriptional program to those active upon differentiation (Supplementary Fig. 7b–g).

Finally, to test the role of H3.3 phosphorylation during enhancer activation, we performed EB differentiation using our exogenous addback system. Expression of the phosphomimic H3.3S31E in H3.3 KO cells resulted in higher H3K27ac at EB enhancers than any other exogenous protein, including H3.3S31A (Fig. 4d and Supplementary Fig. 8a). Accordingly, H3.3S31E expression resulted in increased transcription from differentiation-specific genes and improved EB morphology compared to H3.3S31A expression (Fig. 4e and Supplementary Fig. 8b). Interestingly, expression of the constitutive phosphomimic H3.3S31E during differentiation also perpetuated H3K27ac at mESC-specific enhancers (Supplementary Fig. 8c), supporting our hypothesis that H3.3 phosphorylation promotes enhancer acetylation (Supplementary Fig. 8d).

Collectively, we show that H3.3 is functionally linked to enhancer acetylation in both mESCs and differentiating cells (Supplementary Note). We were surprised that loss of H3.3 in mESCs did not affect p300 recruitment, but rather impacted p300 enzymatic activity, and further, in *trans*. While our data indicate that H3.3 deposition alone may stimulate p300, we observe that mimicking H3.3 phosphorylation allows p300 to enzymatically function to greater potential. Coupled with our *in vitro* observations, we propose that phosphorylation of H3.3S31, in addition to other potentially phosphorylated residues that are common to both canonical and variant H3, provide a “phosphothreshold” for p300 stimulation. In this scenario, H3.3 represents a nucleosomal cofactor for p300 that, through its deposition and phosphorylation, acts to integrate signaling information into chromatin to promote robust enhancer acetylation (Fig. 3d). This model is complementary to other proposed mechanisms of p300 activation, including autoacetylation and signal-mediated transcription factor dimerization<sup>33,34</sup>.

H3.3S31 phosphorylation has previously been reported only during mitosis or enriched at repeat regions such as telomeres<sup>17–19</sup>. Notably, our model is supported by our observation of H3.3S31ph enrichment at mESC enhancers and by a reported role for H3.3S31ph during gene activation<sup>35</sup>. In addition, Chk1, the reported H3.3S31 kinase<sup>19</sup>, has been implicated in gene regulation through histone phosphorylation, supporting a role for this cell-cycle kinase in mediating gene activation<sup>36</sup>. Finally, binding of an H3.3 lysine 36 reader and elongation factor has been shown to be directly affected by serine 31 phosphorylation<sup>37,38</sup>, suggesting an important role for H3.3S31ph in guiding transcription.

Taken together, our study highlights a functional role for H3.3 in gene regulation and also offers important insights towards our understanding of how point mutations to this histone variant influence human disease<sup>20,21</sup>.

## METHODS

### mESC Culture.

Mouse embryonic stem cell lines (mESCs) were cultured on gelatin-coated plates under standard serum/LIF conditions at 37 °C with 5% CO<sub>2</sub> (KO-DMEM, 2 mM Glutamax, 15% ES grade fetal bovine serum, 0.1 mM 2-mercaptoethanol, 1× Pen/Strep, 1× NEAA and leukemia inhibitory factor (LIF)). During thawing and early passages, cells were maintained on an irradiated feeder layer. To remove feeders, cells were passaged at least two passages off of feeders onto gelatin-coated plates. Generation of H3.3 KO<sup>4</sup>, ATRX KO<sup>6</sup>, DAXX KO<sup>6</sup>, and HIRA KO<sup>39</sup> mESCs have been described previously, while HIRA KO2 was generated in our laboratory using CRISPR-Cas9 genome editing. mESCs were routinely tested for mycoplasma.

### Generation of HIRA KO using CRISPR/Cas9.

HIRA KO2 was generating using a lentiCRISPR v2 plasmid (Addgene #52961) containing HIRA guide RNAs (gRNAs) (Supplementary Table 1). 5 µg lentiCRISPR v2 vector, 5 µg psPAX2, and 0.5 µg VSVG plasmids were transfected in serum-free media into  $3 \times 10^6$  293T cells in a 10 cm<sup>2</sup> tissue culture dish using Lipofectamine 3000. Lentivirus-containing supernatants were harvested 48 and 72 h post-transfection, pooled, and concentrated 10× with Lenti-X (Clontech, 63123).  $2 \times 10^5$  mESCs were transduced with 0.2 ml concentrated virus and 8 µg/ml polybrene for 24 h followed by selection with 1 µg/ml puromycin for 3 days. Single cells were isolated by cell sorting. Genotyping of individual clones confirmed deletion and immunoblot confirmed loss of protein.

### Antibodies.

H3 general (ab1791, Abcam, Lot # GR177884–2), H3.3 (09–838, Millipore, Lot # 2578126), H3K4me1 (ab8895, Abcam, Lot # GR193882–2), H3K27ac (39133, Active Motif, Lot # 31814008), H3K27ac (39685, Active Motif, Lot # 14517014), H3K18ac (ab1191, Abcam, Lot # GR3211480–1), H3K64ac (ABE1057, Millipore, Lot # 2826017), H3K122ac (ab33309, Abcam, Lot # GR284790–3), Spike-In antibody (61686, Active Motif, Lot# 00419007), H3.1/2 (ABE154, Millipore), p300 (sc-584, Santa Cruz, Lot # F3016), Gapdh (2118, Cell Signaling, Lot # 10), Lamin A (ab26300, Abcam, Lot # GR155781–1), b-Tubulin (T5201, Sigma, Lot # 088K4832), H3S10ph (39253, Active Motif, Lot # 8308001), H3S28ph (07–145, Millipore, Lot # 27707), H3S31ph (ab92628, Abcam, Lot # GR296764–8), HIRA (WC15/WC119 hybridoma), DAXX (07–471, Millipore, Lot # 2841952), ATRX (ab97508, Abcam, Lot # GR267227–8), Oct4 (sc-5279, Santa Cruz, Lot # C3109), anti-mouse IgG-HRP (NA93V, GE, Lot # 9773218), anti-rabbit IgG-HRP (170–6515, Biorad, Lot # 350003248).

### Chromatin Immunoprecipitation (ChIP).

Native and crosslinking (X) ChIP were performed with  $5 \times 10^6$  and  $6 \times 10^7$  cells, respectively, as previously described<sup>2</sup>. A spike-in normalization strategy was used to normalize all ChIP-seq data to reduce the effects of technical variation and sample

processing bias. Spike-In chromatin (Active Motif, 53083) and Spike-in antibody (Active Motif, 61686) were used according to manufacturer instructions.

**Native ChIP.**—Cells were trypsinized, washed and subjected to hypotonic lysis (50 mM TrisHCl pH 7.4, 1 mM CaCl<sub>2</sub>, 0.2% Triton X-100, 10 mM NaButyrate, and protease inhibitor cocktail (Roche)) with micrococcal nuclease for 5 min at 37 °C to recover mono- to tri-nucleosomes. Nuclei were lysed by brief sonication and dialyzed into RIPA buffer (10 mM Tris pH 7.6, 1 mM EDTA, 0.1% SDS, 0.1% Na-Deoxycholate, 1% Triton X-100) for 2 h at 4 °C. Soluble material was incubated with 3–5 µg of antibody bound to 50 µl protein A or protein G Dynabeads (Invitrogen) and incubated overnight at 4 °C, with 5% reserved as input DNA. Magnetic beads were washed as follows: 3× RIPA buffer, 2× RIPA buffer + 300 mM NaCl, 2× LiCl buffer (250 mM LiCl, 0.5% NP-40, 0.5% NaDeoxycholate), 1× TE + 50 mM NaCl. Chromatin was eluted and treated with RNaseA and Proteinase K. ChIP DNA was purified and dissolved in H<sub>2</sub>O.

**X-ChIP.**—Cells were crosslinked with 1% formaldehyde for 10 min at room temperature and quenched with 0.125 M glycine. Nuclei were resuspended in X-ChIP buffer (10 mM Tris pH 8, 100 mM NaCl, 1 mM EDTA, 0.5 mM EGTA, 0.1% Na-Deoxycholate, 0.5% N-lauroylsarcosine) and chromatin was sonicated to an average size of 0.3–0.7 kb using Covaris M220 Focused-ultrasonicator. Soluble material was incubated with 10 µg of antibody bound to 100 µl protein A or protein G Dynabeads (Invitrogen) and incubated overnight at 4 °C, with 5% reserved as input DNA. Magnetic beads were washed as follows: 1× Low Salt buffer (10 mM TrisHCl pH 8, 2 mM EDTA, 0.1% SDS, 1% Triton X-100, 150 mM NaCl), 1× High Salt buffer (10 mM TrisHCl pH 8, 2 mM EDTA, 0.1% SDS, 1% Triton X-100, 500 mM NaCl), 1× LiCl buffer (10 mM TrisHCl pH 8, 1 mM EDTA, 1% NP-40, 1% NaDeoxycholate, 250 mM LiCl), 1× TE + 50 mM NaCl. Chromatin was eluted and treated with RNaseA and Proteinase K. ChIP DNA was purified and dissolved in H<sub>2</sub>O.

**ChIP-qPCR.**—qPCR was performed in triplicate using a LightCycler® 480 Instrument II system and Power SYBR Green PCR master mix. ChIP DNA samples were diluted 1:50 in H<sub>2</sub>O, with 5 µl used per reaction. ChIP-qPCR signal is represented as percent input. All qPCR primer sequences used in this study are listed in Supplementary Table 1.

## ChIP-seq.

**ChIP-seq Library Preparation.**—ChIP-seq libraries were prepared from 5–10 ng ChIP DNA following the Illumina TruSeq protocol. The quality of the libraries was assessed using a D1000 ScreenTape on a 2200 TapeStation (Agilent) and quantified using a Qubit dsDNA HS Assay Kit (Thermo Fisher). Libraries with unique adaptor barcodes were multiplexed and sequenced on an Illumina NextSeq 500 (paired-end, 33 base pair reads). Typical sequencing depth was at least 20 million reads per sample.

**ChIP-seq Data Quality Control, Alignment and spike-in normalization.**—Quality of ChIP-seq datasets was assessed using the FastQC tool. ChIP-seq raw reads were aligned separately to the mouse reference genome (mm10) and the spike-in *Drosophila* reference genome (dm3) using BOWTIE<sup>40</sup>. Only one alignment is reported for each read (either the

single best alignment or, if more than one equivalent best alignment was found, one of those matches selected randomly). Duplicate reads were filtered using the rmdup function of SAMtools<sup>29</sup>. Uniquely mapped drosophila reads were counted in the sample containing the least number of Drosophila mapped reads and used to generate a normalization factor for random downsampling. Reads were converted into bigWig files using BEDTools<sup>41</sup> for visualization in Integrative Genomics Viewer<sup>42</sup>.

**Peak Calling.**—Peak calling was performed using MACS2 software<sup>43</sup> using cut-off values “--pvalue 1e-2 --mfold 10,50” and input as a control in each replicated sample. Peaks were filtered by peak height to reduce false positives and retain only robust peaks for further analyses.

**Average Profiles.**—Bigwig files were used to generate average ChIP-seq profiles using deepTools.

**Box plots.**—Box plot representations were used to quantitatively assess the read distribution in a fixed window. Box plots are defined by the median, box limits at upper and lower quartiles of 75% and 25%, and whiskers at 90% and 10%. The read distribution surrounding the peak center was calculated and plotted using custom R scripts. Wilcoxon rank sum tests were performed to determine the statistical significance of all comparisons.

**Heatmaps.**—The read densities surrounding 6 kb ( $\pm$  3 kb) of the peak center of p300 peaks (rank ordered by highest to lowest H3K27ac enrichment in WT mESCs) were determined and visualized as heatmaps using deepTools.

**Density plots.**—Density plots representing fold-change differences between samples were generated using custom R scripts. k-s tests were performed to determine the statistical significance of all comparisons.

## ATAC-seq.

ATAC-seq was performed as previously described<sup>29</sup> with minor changes. For each sample, 100,000 cells were harvested, washed and lysed with ATAC buffer (Tris 10 mM pH 7.4, 10 mM NaCl, 3 mM MgCl<sub>2</sub>, NP-40 0.1%). Nuclei were collected and subject to tagmentation 37 °C for 30 minutes. Reaction was stopped with 0.2% SDS and DNA was collected using Qiaquick PCR purification columns and eluted in 10  $\mu$ l 10 mM Tris, pH 8. Eluted DNA was amplified using KAPA non-hot-start PCR kit and purified using AMPure XP beads (negative and positive selection). Samples were pooled for multiplexing and sequenced using paired-end sequencing on the Illumina NextSeq 500.

**ATAC-seq Data Quality Control, Alignment and normalization.**—Quality of the ATAC-seq datasets was assessed using the FastQC tool. The ATAC-seq reads were then aligned to the mouse reference genome (mm10) using BWA<sup>2</sup>. For unique alignments, duplicate reads were filtered out. The resulting uniquely mapped reads were normalized to the same read depth across all samples and converted into bigWig files using BEDTools<sup>41</sup> for visualization in Integrative Genomics Viewer<sup>42</sup>. Heatmaps were generated using deepTools.

### Addback Experiments.

pCDH-EF1a-H3-Flag-HA-IRES-Neo constructs containing histone mutations were made using site-directed mutagenesis followed by Sanger sequencing to confirm the mutations (H3.2 and H3.3 sequences are listed in Supplementary Table 1). Lentivirus was packaged in 293T cells as described above.  $2 \times 10^5$  WT and H3.3 KO mESCs were incubated with 0.2 ml concentrated lentivirus and polybrene (8  $\mu$ g/ml). The next day, the medium was replaced with complete mESC culture medium containing 300  $\mu$ g/ml G418. After 4 days of selection, mESCs were used for downstream analysis.

### shRNA transduction.

For p300 and CBP knockdown, (Dharmacon) plasmids were packaged as described above.  $2 \times 10^5$  WT mESCs were incubated with 0.2 ml concentrated lentivirus and polybrene (8  $\mu$ g/ml). The next day, the medium was replaced with complete mESC culture medium containing 1  $\mu$ g/ml puromycin. After 4 days of selection, mESCs were used for western blot analysis.

### In Vitro Phosphorylation and HAT assay.

Full length p300 was expressed in Sf9 cells and purified with 3 $\times$ FLAG beads. Both recombinant human CHK1 protein and recombinant mononucleosomes were purchased from Active Motif (31163, 81070). First, H3.3 mononucleosomes were incubated with CHK1 (50 ng) in kinase buffer (50 mM Tris-HCl pH 7.4, 10 mM MgCl<sub>2</sub>, 1 mM DTT, 5% glycerol, protease inhibitor cocktail) in the presence or absence of 0.2 mM ATP at 37 °C for 5 min. The reaction was terminated by the addition of 5  $\mu$ M CHK1 inhibitor SB218078 (Tocris, Cat. No. 2560). Immediately, the HAT assay was performed by adding 25  $\mu$ M acetyl-CoA (<sup>3</sup>H AcetylCOA in the case of HOT reaction), 100 ng of full length p300 (plus H3.1 mononucleosomes in case of the *trans* assay) for 30 min at 30 °C. The reaction was stopped by adding SDS sample buffer and the samples were subject to downstream analysis (immunoblot analysis, autoradiography, mass spectrometry).

### Colony Formation Assay.

WT and H3.3 KO mESCs were seeded at a density of 100 cells/well in 6 well-plates. Medium was changed every 2–3 days. For all experiments, seven days after initial seeding, cells were fixed and stained using the Alkaline Phosphatase Staining Kit (STEMGENT, 00–0055). Colonies were scored manually in a blinded fashion as undifferentiated, differentiated, or mixed.

### Quantitative RT-PCR and mRNA-seq.

mRNA was isolated using QIAGEN RNeasy. 500 ng of total RNA was reverse transcribed using random hexamers and MultiScribe reverse transcriptase. mRNA expression was analyzed by quantitative PCR (qPCR) with SYBR Green using a LightCycler 480 (Roche). All qPCR primer sequences used in this study are listed in Supplementary Table 1.

For RNA-seq, total mRNA from equal cell numbers was mixed with synthetic RNA standards (ERCC RNA Spike-In Mix, Thermo Fisher)<sup>44</sup>. Libraries were prepared according

to the Illumina TruSeq protocol and sequenced on an Illumina NextSeq 500 (paired-end, 33 base pair reads).

### Analysis of RNA-seq Data.

**Data Quality Control, Alignment and normalization.**—Quality of the RNA-seq raw reads was assessed using the FastQC tool. The reads were then aligned to the mouse reference genome (mm10) and the spike-in control ERCC92 using TopHat<sup>45</sup>. Reads mapping to ERCC92 were counted using htseq-count<sup>46</sup> and used to normalize the counts to genes. After normalization, the reads were converted into bigWig files using BEDTools for visualization in Integrative Genomics Viewer<sup>42</sup> or the UCSC genome browser<sup>41</sup>.

**Differential Expression Analysis (DE).**—Gene expression level measured as FPKM was determined by the maximum likelihood estimation method implemented in the Cufflinks software package with annotated transcripts as references. Differential expression was analyzed using the Student's *t* test in the program Cuffdiff<sup>45</sup> with *P* values corrected for multiple testing.

**Venn Diagrams.**—To check the extent of overlap of the up- and downregulated genes from RNA-seq with the nearest neighbor genes of the ChIP-seq peaks (obtained from GREAT software), Venn diagrams were generated using custom R scripts.

**MA Plots.**—MA plots were used to graphically represent genes that were upregulated or downregulated by more than 2-fold. The log<sub>2</sub> fold change (KO/WT) was plotted on the y-axis versus the log<sub>2</sub> mean of normalized counts on the x-axis.

### Embryoid Body Differentiation Assay.

mESCs were dissociated to form a single-cell suspension. The cells were diluted to  $1 \times 10^4$  cells/ml in EB differentiation media (DMEM, 15% FBS, 1× MEM-NEAA, 1× Penicillin-Streptomycin, 50 μM β-mercaptoethanol) and  $100 \times 30 \mu\text{l}$  drops were placed on the lid of a 150 mm dish. The lid was carefully inverted and placed over a bottom dish containing 10–15 ml of PBS. The hanging drops were cultured for 3 days in 5% CO<sub>2</sub> at 37 °C. On the third day the hanging drops were washed from the lids with EB differentiation media and culture was continued in 100 mm dishes in 5% CO<sub>2</sub> at 37 °C on an orbital shaker at 50 rpm for up to 12 days (culture media was changed every other day).

**EB ChIP.**—H3K27ac Native ChIP was performed on day 4 EB (15 and 40 15-cm<sup>2</sup> dishes of wild-type and H3.3 null EB, respectively). EB were pooled and incubated for 10 min on ice in 0.5 ml hypotonic lysis buffer with protease inhibitor cocktail (50 mM Tris-HCl pH 7.6, 1 mM CaCl<sub>2</sub>, 0.2% Triton X-100). Tubes were inverted intermittently during the incubation to aid lysis. After the lysates were treated with MNase for 5 min in a 37 °C water bath, Native ChIP continued as described above.

### Quantification and Statistical Analysis.

To check the significance of all comparisons, Wilcoxon rank sum test was used to calculate *P* values for data used to generate boxplots. Two-sample Kolmogorov-Smirnov test was used

to calculate *P* values to show significant changes between two density curves. ANOVA test was used for two or more independent comparison groups.

### Reporting Summary.

Further information on research design is available in the Life Sciences Reporting Summary linked to this article.

### Code Availability.

Code to generate figures is available at <https://github.com/utsw-medical-center-banaszynski-lab/Martire-et-al-2019-Nature-Genetics.git>

### Data Availability.

Datasets are deposited in the NCBI Gene Expression Omnibus using the following accession numbers: SuperSeries GSE114551, ATAC-seq GSE114547, ChIP-seq GSE114548, and RNA-seq GSE114549.

### Supplementary Material

Refer to Web version on PubMed Central for supplementary material.

### Acknowledgments

We thank members of the Banaszynski and Hon laboratories for helpful discussions; E. Duncan, H. Yu, L. Kraus, H. Zhu, and S. Morrison for critical comments on this manuscript; A. Shoshnev for the illustrations used as templates in this manuscript; UTSW BioHPC for computational infrastructure; UTSW McDermott Center and the Children's Research Institute for providing next-generation sequencing services; UTSW Flow Cytometry Core for single cell isolation; UTSW Proteomics Core for mass spectrometry analysis. L.A.B. is a Virginia Murchison Linthicum Scholar in Medical Research (UTSW Endowed Scholars Program) and a Peterson Investigator of the Neuroendocrine Research Foundation (NETRF). This work was supported in part by CPRIT RR140042, The Welch Foundation I-1892, DoD KCRP KC170230, and NIH R35 GM124958 (L.A.B.), the American-Italian Cancer Foundation (S.M.), the Taiwan Postdoctoral Research Abroad Fellowship (Y.-C.T), and the Green Center for Reproductive Biology Sciences.

### REFERENCES

1. Shi L, Wen H & Shi X The Histone Variant H3.3 in Transcriptional Regulation and Human Disease. *J. Mol. Biol* 429, 1934–1945 (2017). [PubMed: 27894815]
2. Goldberg AD et al. Distinct factors control histone variant H3.3 localization at specific genomic regions. *Cell* 140, 678–691 (2010). [PubMed: 20211137]
3. Wong LH et al. ATRX interacts with H3.3 in maintaining telomere structural integrity in pluripotent embryonic stem cells. *Genome Res.* 20, 351–360 (2010). [PubMed: 20110566]
4. Banaszynski LA et al. Hira-dependent histone H3.3 deposition facilitates PRC2 recruitment at developmental loci in ES cells. *Cell* 155, 107–120 (2013). [PubMed: 24074864]
5. Elsässer SJ, Noh K-M, Diaz N, Allis CD & Banaszynski LA Histone H3.3 is required for endogenous retroviral element silencing in embryonic stem cells. *Nature* 522, 240–244 (2015). [PubMed: 25938714]
6. Sadic D et al. Atrx promotes heterochromatin formation at retrotransposons. *EMBO Rep.* (2015). doi:10.15252/embr.201439937
7. He Q et al. The Daxx/Atrx Complex Protects Tandem Repetitive Elements during DNA Hypomethylation by Promoting H3K9 Trimethylation. *Cell Stem Cell* 17, 273–286 (2015). [PubMed: 26340527]

8. Voon HPJ et al. ATRX Plays a Key Role in Maintaining Silencing at Interstitial Heterochromatic Loci and Imprinted Genes. *Cell Rep* 11, 405–418 (2015). [PubMed: 25865896]
9. Jang C-W, Shibata Y, Starmer J, Yee D & Magnuson T Histone H3.3 maintains genome integrity during mammalian development. *Genes Dev.* 29, 1377–1392 (2015). [PubMed: 26159997]
10. Hödl M & Basler K Transcription in the absence of histone H3.3. *Curr. Biol* 19, 1221–1226 (2009). [PubMed: 19523831]
11. Sakai A, Schwartz BE, Goldstein S & Ahmad K Transcriptional and developmental functions of the H3.3 histone variant in *Drosophila*. *Curr. Biol* 19, 1816–1820 (2009). [PubMed: 19781938]
12. Kim H, Heo K, Choi J, Kim K & An W Histone variant H3.3 stimulates HSP70 transcription through cooperation with HP1 $\gamma$ . *Nucleic Acids Res.* 39, 8329–8341 (2011). [PubMed: 21742762]
13. Tamura T et al. Inducible deposition of the histone variant H3.3 in interferon-stimulated genes. *J. Biol. Chem* 284, 12217–12225 (2009). [PubMed: 19244243]
14. Zhang H et al. RPA Interacts with HIRA and Regulates H3.3 Deposition at Gene Regulatory Elements in Mammalian Cells. *Mol. Cell* 65, 272–284 (2017). [PubMed: 28107649]
15. Nashun B et al. Continuous Histone Replacement by Hira Is Essential for Normal Transcriptional Regulation and De Novo DNA Methylation during Mouse Oogenesis. *Mol. Cell* 60, 611–625 (2015). [PubMed: 26549683]
16. Kong Q et al. Histone variant H3.3-mediated chromatin remodeling is essential for paternal genome activation in mouse preimplantation embryos. *J. Biol. Chem* jbc.RA117.001150 (2018). doi:10.1074/jbc.RA117.001150
17. Wong LH et al. Histone H3.3 incorporation provides a unique and functionally essential telomeric chromatin in embryonic stem cells. *Genome Res.* 19, 404–414 (2009). [PubMed: 19196724]
18. Hake SB et al. Serine 31 phosphorylation of histone variant H3.3 is specific to regions bordering centromeres in metaphase chromosomes. *Proc. Natl. Acad. Sci. U.S.A.* 102, 6344–6349 (2005). [PubMed: 15851689]
19. Chang FTM et al. CHK1-driven histone H3.3 serine 31 phosphorylation is important for chromatin maintenance and cell survival in human ALT cancer cells. *Nucleic Acids Res.* 43, 2603–2614 (2015). [PubMed: 25690891]
20. Schwartzentruber J et al. Driver mutations in histone H3.3 and chromatin remodelling genes in paediatric glioblastoma. *Nature* 482, 226–231 (2012). [PubMed: 22286061]
21. Behjati S et al. Distinct H3F3A and H3F3B driver mutations define chondroblastoma and giant cell tumor of bone. *Nat. Genet* 45, 1479–1482 (2013). [PubMed: 24162739]
22. Pasini D et al. Characterization of an antagonistic switch between histone H3 lysine 27 methylation and acetylation in the transcriptional regulation of Polycomb group target genes. *Nucleic Acids Res.* 38, 4958–4969 (2010). [PubMed: 20385584]
23. Chen X et al. Integration of external signaling pathways with the core transcriptional network in embryonic stem cells. *Cell* 133, 1106–1117 (2008). [PubMed: 18555785]
24. Pradeepa MM et al. Histone H3 globular domain acetylation identifies a new class of enhancers. *Nat. Genet* 48, 681–686 (2016). [PubMed: 27089178]
25. Dorigi KM et al. Mll3 and Mll4 Facilitate Enhancer RNA Synthesis and Transcription from Promoters Independently of H3K4 Monomethylation. *Mol. Cell* 66, 568–576.e4 (2017). [PubMed: 28483418]
26. Rickels R et al. Histone H3K4 monomethylation catalyzed by Trr and mammalian COMPASS-like proteins at enhancers is dispensable for development and viability. *Nat. Genet* 49, 1647–1653 (2017). [PubMed: 28967912]
27. Lai B et al. MLL3/MLL4 are required for CBP/p300 binding on enhancers and super-enhancer formation in brown adipogenesis. *Nucleic Acids Res.* (2017). doi:10.1093/nar/gkx234
28. Wang C et al. Enhancer priming by H3K4 methyltransferase MLL4 controls cell fate transition. *Proc. Natl. Acad. Sci. U.S.A.* 113, 11871–11876 (2016). [PubMed: 27698142]
29. Buenrostro JD, Giresi PG, Zaba LC, Chang HY & Greenleaf WJ Transposition of native chromatin for fast and sensitive epigenomic profiling of open chromatin, DNA-binding proteins and nucleosome position. *Nat. Methods* 10, 1213–1218 (2013). [PubMed: 24097267]

30. Josefowicz SZ et al. Chromatin Kinases Act on Transcription Factors and Histone Tails in Regulation of Inducible Transcription. *Mol. Cell* 64, 347–361 (2016). [PubMed: 27768872]
31. Cheung P et al. Synergistic coupling of histone H3 phosphorylation and acetylation in response to epidermal growth factor stimulation. *Mol. Cell* 5, 905–915 (2000). [PubMed: 10911985]
32. Li M, Dong Q & Zhu B Aurora Kinase B Phosphorylates Histone H3.3 at Serine 31 during Mitosis in Mammalian Cells. *J. Mol. Biol* 429, 2042–2045 (2017). [PubMed: 28137420]
33. Delvecchio M, Gaucher J, Aguilar-Gurrieri C, Ortega E & Panne D Structure of the p300 catalytic core and implications for chromatin targeting and HAT regulation. *Nat. Struct. Mol. Biol* 20, 1040–1046 (2013). [PubMed: 23934153]
34. Ortega E et al. Transcription factor dimerization activates the p300 acetyltransferase. *Nature* 562, 538–544 (2018). [PubMed: 30323286]
35. Thorne JL, Ouboussad L & Lefevre PF Heterochromatin protein 1 gamma and IκB kinase alpha interdependence during tumour necrosis factor gene transcription elongation in activated macrophages. *Nucleic Acids Res.* 40, 7676–7689 (2012). [PubMed: 22649058]
36. Shimada M et al. Chk1 is a histone H3 threonine 11 kinase that regulates DNA damage-induced transcriptional repression. *Cell* 132, 221–232 (2008). [PubMed: 18243098]
37. Guo R et al. BS69/ZMYND11 reads and connects histone H3.3 lysine 36 trimethylation-decorated chromatin to regulated pre-mRNA processing. *Mol. Cell* 56, 298–310 (2014). [PubMed: 25263594]
38. Wen H et al. ZMYND11 links histone H3.3K36me3 to transcription elongation and tumour suppression. *Nature* 508, 263–268 (2014). [PubMed: 24590075]
39. Roberts C et al. Targeted mutagenesis of the Hira gene results in gastrulation defects and patterning abnormalities of mesoendodermal derivatives prior to early embryonic lethality. *Mol. Cell. Biol* 22, 2318–2328 (2002). [PubMed: 11884616]
40. Langmead B, Trapnell C, Pop M & Salzberg SL Ultrafast and memory-efficient alignment of short DNA sequences to the human genome. *Genome Biol.* 10, R25 (2009). [PubMed: 19261174]
41. Quinlan AR & Hall IM BEDTools: a flexible suite of utilities for comparing genomic features. *Bioinformatics* 26, 841–842 (2010). [PubMed: 20110278]
42. Robinson JT et al. Integrative genomics viewer. *Nat. Biotechnol* 29, 24–26 (2011). [PubMed: 21221095]
43. Zhang Y et al. Model-based analysis of ChIP-Seq (MACS). *Genome Biol.* 9, R137 (2008). [PubMed: 18798982]
44. Jiang L et al. Synthetic spike-in standards for RNA-seq experiments. *Genome Res.* 21, 1543–1551 (2011). [PubMed: 21816910]
45. Trapnell C, Pachter L & Salzberg SL TopHat: discovering splice junctions with RNA-Seq. *Bioinformatics* 25, 1105–1111 (2009). [PubMed: 19289445]
46. Anders S, Pyl PT & Huber W HTSeq--a Python framework to work with high-throughput sequencing data. *Bioinformatics* 31, 166–169 (2015). [PubMed: 25260700]

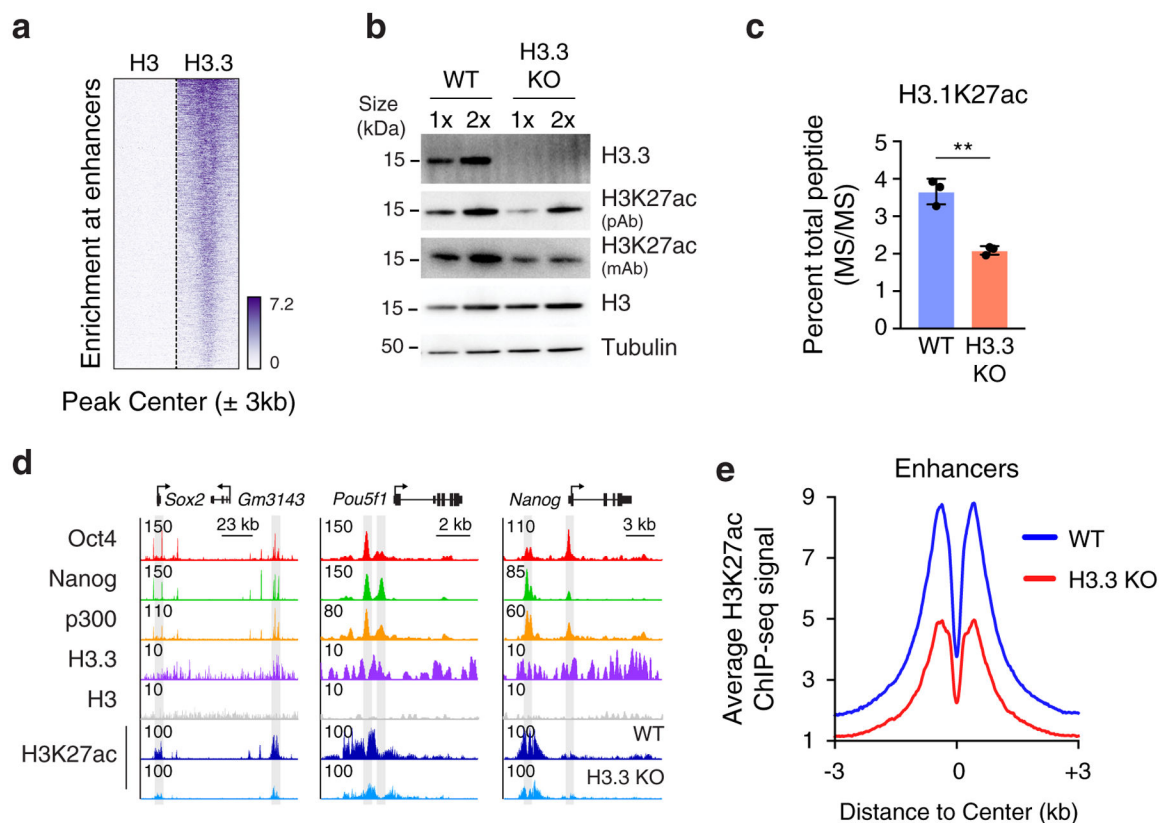


**Figure 1. Histone H3.3 facilitates histone acetylation at enhancers.**

**a**, Heatmap showing enrichment of H3 and H3.3 at promoter-distal enhancers ( $\pm 3$  kb from TSS) in mESCs. Each row represents a single enhancer ( $n = 17,589$ ).

**b**, Immunoblot with the indicated antibodies from WT and H3.3 KO mESC whole-cell lysates loaded with increased protein concentration (1 $\times$ , 2 $\times$ ). Blot is representative of more than five independent experiments. See also Supplementary Figure 9a.

**c**, Quantification of H3.1K27 acetylation levels in WT and H3.3 KO mESCs by mass spectrometry (Mod Spec<sup>TM</sup>, Active Motif). Data are represented as percent of the total H3.1(27–41) peptide observed,  $n = 3 \pm$  s.d., two-tailed  $t$  test, \*\*  $P$  value = 0.0071.

**d**, Genome browser representations of Oct4, Nanog, p300, H3.3 and H3 ChIP-seq in WT mESCs and of H3K27ac ChIP-seq in WT and H3.3 KO mESCs. The y-axis represents read density in reads per kilobase per million mapped reads (RPKM) normalized to an external standard. Gray boxes indicate regulatory elements. Data are representative of three independent experiments using two different antibodies.

**e**, ChIP-seq average profiles in WT and H3.3 KO mESCs of H3K27ac at enhancers.

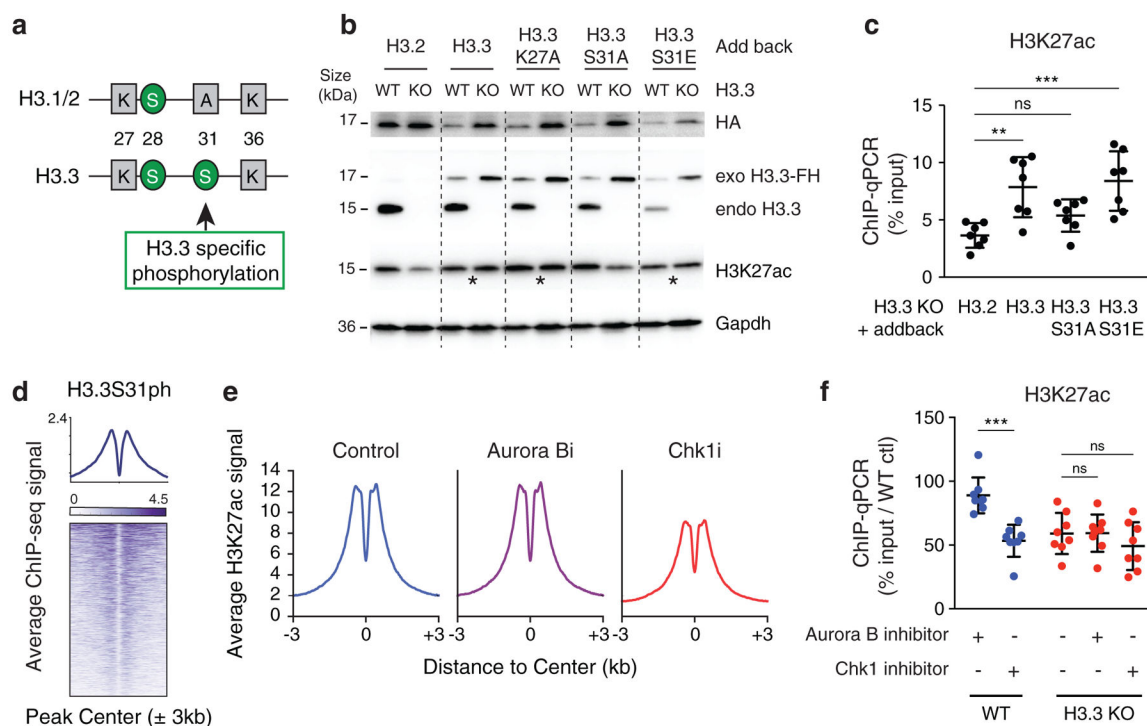


**Figure 2. H3.3 phosphorylation promotes acetylation at enhancers**

**a**, Schematic of the histone H3.1/2 and H3.3 tails, highlighting the site of H3.3-specific phosphorylation.

**b**, Immunoblot of whole-cell lysates from WT and H3.3 KO mESCs exogenously expressing histones and indicated mutant histones. \* indicates similar H3K27ac levels in WT and KO addback comparisons. Blot is representative of three independent experiments. See also Supplementary Figure 9b.

**c**, ChIP-qPCR of H3K27ac enrichment at enhancer regions (n = 7) in H3.3 KO mESCs exogenously expressing histones and indicated mutant histones. Data are normalized to input and represent mean  $\pm$  s.d., ordinary one-way ANOVA test, \*\*  $P=0.0022$ , \*\*\*  $P=0.0007$ , n.s. = 0.28

**d**, ChIP-seq heatmap and average profile of H3.3S31ph at enhancers. Each row represents a single enhancer (n = 17,589).

**e**, ChIP-seq average profiles of H3K27ac at enhancers in WT mESCs treated with Aurora B or Chk1 inhibitors for 4 hours.

**f**, ChIP-qPCR of H3K27ac at enhancer regions (n = 8) in WT and H3.3 KO mESCs Aurora B or Chk1 inhibitors for 4 hours. Data are normalized to WT control and represent mean  $\pm$  s.d., ordinary one-way ANOVA test, \*\*\*  $P=0.0002$ , n.s. = 0.9, n.s. = 0.4.

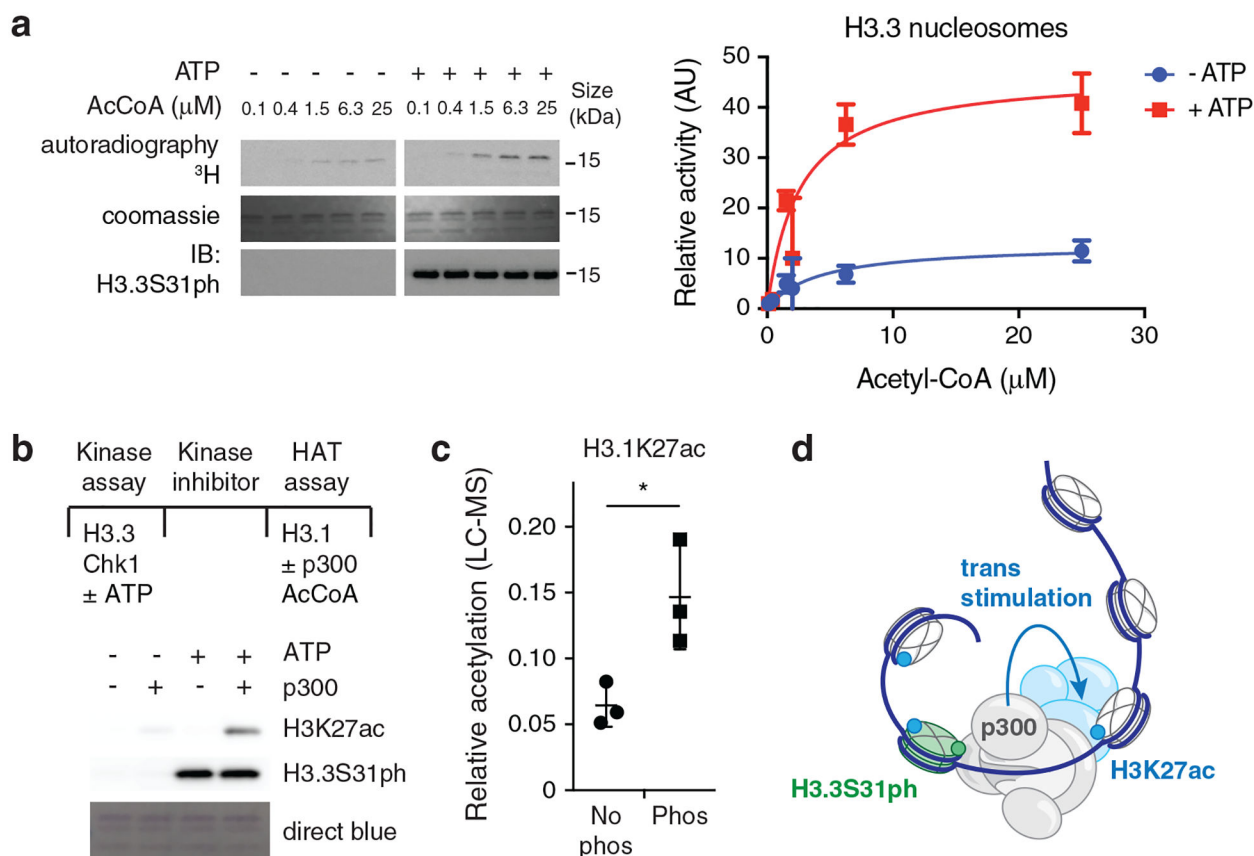


**Figure 3. H3.3 phosphorylation stimulates p300 histone acetyltransferase activity in *trans***

**a**, p300 histone acetyltransferase assay using recombinant H3.3 nucleosomes that were preincubated with Chk1 with or without ATP. Representative autoradiography, commassie, and immunoblot are shown on the left. Quantification of histone acetylation is shown on the right, represented as mean (n = 3) ± s.d.

**b**, p300 histone acetyltransferase assay using recombinant H3.3 nucleosomes treated as indicated with recombinant H3.1 nucleosomes as substrates. Blot is representative of three independent experiments. See also Supplementary Figure 9c.

**c**, Related to panel b. Quantification of H3.1K27ac levels by mass spectrometry. Data are normalized to the total amount of H3.1 peptide observed. n = 3 ± s.d. two-tailed *t* test, \* *P* = 0.029

**d**, Model figure representing H3.3S31ph stimulation of p300 activity in *trans*.

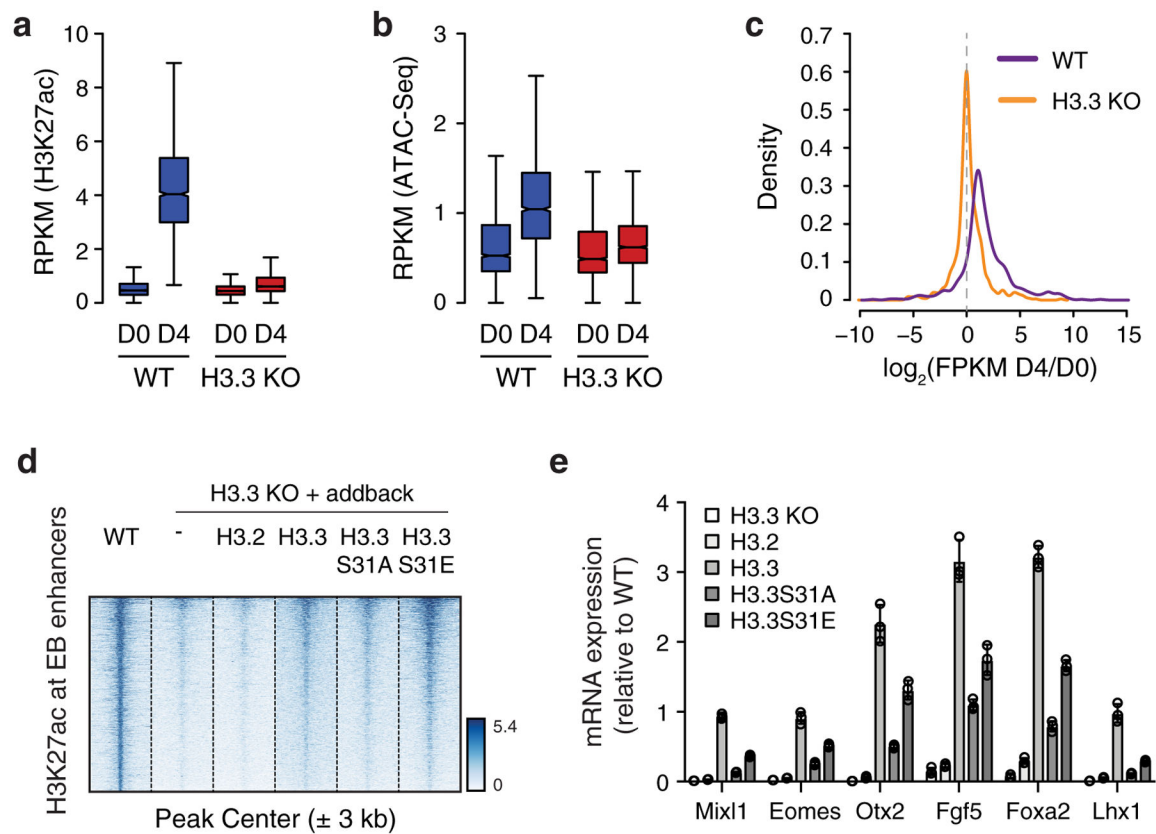


**Figure 4. H3.3 Phosphorylation promotes the establishment of new enhancers during differentiation.**

**a**, Boxplot showing H3K27ac enrichment at enhancers acetylated after 4 days of differentiation ( $n = 2,054$ ) in WT and H3.3 KO day 4 EBs.  $P < 2.2 \times 10^{-16}$  for all comparisons by Wilcoxon rank sum two-side test. The bottom and top of the boxes correspond to the 25<sup>th</sup> and 75<sup>th</sup> percentiles, and the internal band is the 50<sup>th</sup> percentile (median). The plot whiskers correspond to  $1.5 \times$  interquartile range and outliers are excluded.

**b**, Boxplot showing ATAC-seq at enhancers acetylated after 4 days of differentiation ( $n = 2,054$ ) in WT and H3.3 KO day 4 EBs.  $P < 2.2 \times 10^{-16}$  for all comparisons by Wilcoxon rank sum two-side test. Boxplots displayed as in panel a.

**c**, Ratio ( $\log_2$ ) of RNA expression from nearby genes of differentiation-specific enhancers ( $n = 1,840$ ) in day 4 EBs versus mESCs for WT and H3.3 KO cells. x axis values  $> 0$  indicate increased gene expression upon differentiation.  $P < 2.2 \times 10^{-16}$  between WT and H3.3 KO curves by Kolmogorov-Smirnov test.

**d**, Heatmap of H3K27ac enrichment in WT and H3.3 KO cells expressing exogenous histone mutants at day 4 at differentiation-specific enhancers. 3 kb around the center of enhancers are displayed for each analysis. Each row represents a single enhancer ( $n = 2,054$ ).

**e**, RT-qPCR analysis of differentiation-specific genes of day 4 EBs in H3.3 KO cells expressing exogenous histone mutants. Data represented as mean  $\pm$  s.d ( $n = 3$ ).